Pre-Analysis Report

Final calibration GI beamline (1-30nm)

PROBA-2 / LYRA

15-17 March 2006

Doc. RP-ROB-LYR-0132-GI-March2006

issue Version 1.0
09 May 2006

Prepared by : A. BEN MOUSSA (ROB)
Verified by :
Released by :

Distribution List

Recipients	Affiliation	Nr. of Copies
LYRA team	CSL, IMO, PMOD, MPS, IEMN, ROB	Email copy

Document Change Record

Issue	Date	Comments

Table of Contents

Reference documents

[RD1] : Final_LYRA_GI_Instrument_Calibration_Plan-V1.1.doc (ROB: 09/03/2006)

[RD2] : LYRA_Assembly_270705.xls (PMOD)

[RD3] : RP-ROB-LYR-0132-GI-July2005

Scope

The purpose of this report is to summarize results from the GI calibration at PTB-Bessy II (2006).

1 Execution Plan for LYRA

For more details, see [RD1]. The PTB campaign plan was executed as following:

Activities number	Activities name	Remark
1	Linearity vs Flux at $\lambda_{1 \text{ or } 2}$	See RD1
2	Stability vs Time at $\lambda_{1 \text{ or } 2}$	"
3	Spectral responsivity [1-30 nm]	"
4	Raster Scan at $\lambda_{1 \text{ or } 2}$	"
5	VIS-Leds testing (On-Off)	"
6	Signal vs Integration time LYRA	"

All tests were performed around 37°C (LYRA foot sensor) and measured at **10nm** for Zr channels (1-4, 2-4 and 3-4) and at **18nm** for Al channels (1-3, 2-3 and 3-3).

The linearity was investigated using different aperture stops or by varying the exit slit of the respective monochromator.

For the signal stability, the shutter was opened and closed every 60s (short stability) then every 600s (long). Each shutter movement resets the timescale. Some "extra" tests were carried out. The expected beam power was calculated using the responsivity data.

The responsivity was measured in the center position at regular intervals and in finest steps close to C absorption and Al filter cut-off.

Raster scan was normalized to the value of the centre point to aid comparison. The beamline power has been readjusted between scans to better conform to detector sensitivities. Note that the full beam size (0.3 x 0.3 mm) on the measured profile can be negligible.

Voltage units were changed to current units (nA) using the appropriate gain resistor [see RD2]. Corrections for the small decline of the current of the synchrotron storage ring during the time period of each measurement have been applied by ROB.

For clarity, we did not plot the estimated error bars to the data .

2 RESULTS

2.1 Channel 1-3 (Head 1 ; Channel 3: Al, MSM11)

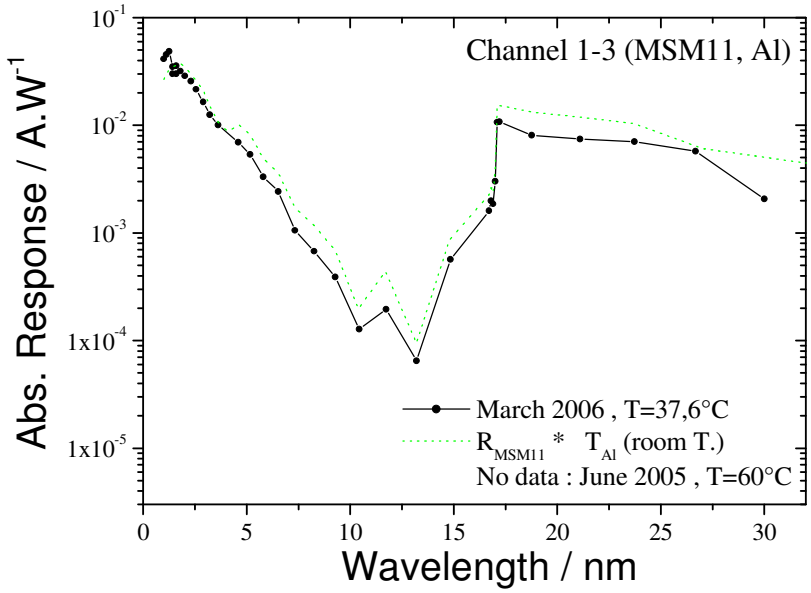

Figure 1. Absolute spectral responsivity (in A/W) of channel 1-3 between 1nm and 30 nm. For comparison, the dotted line represents the model used in the LYRA radiometric model (detector R x Filter T).

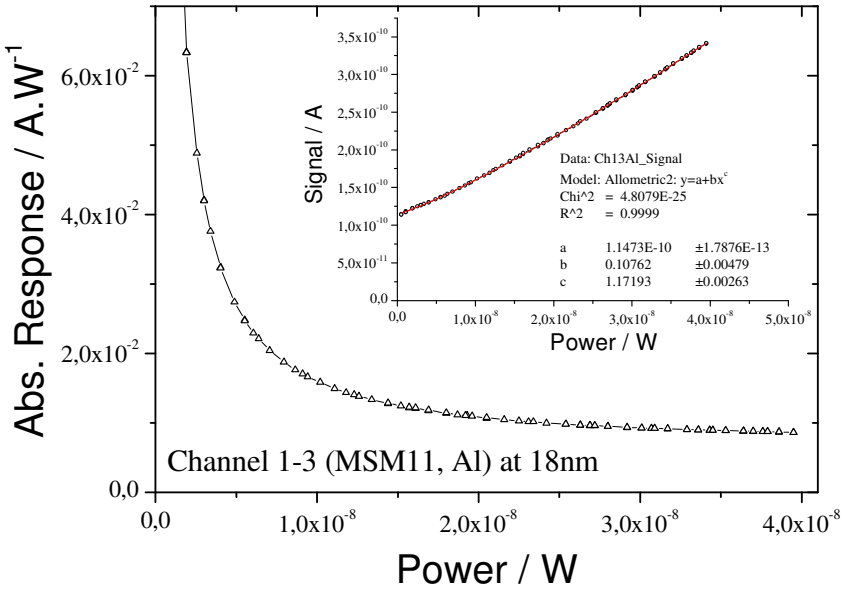

Figure 2. Flux linearity of channel 1-3 (Response vs. incident power) at 18nm. The inset shows the photocurrent vs incident power with the fitted function $I=a+bP^c$.

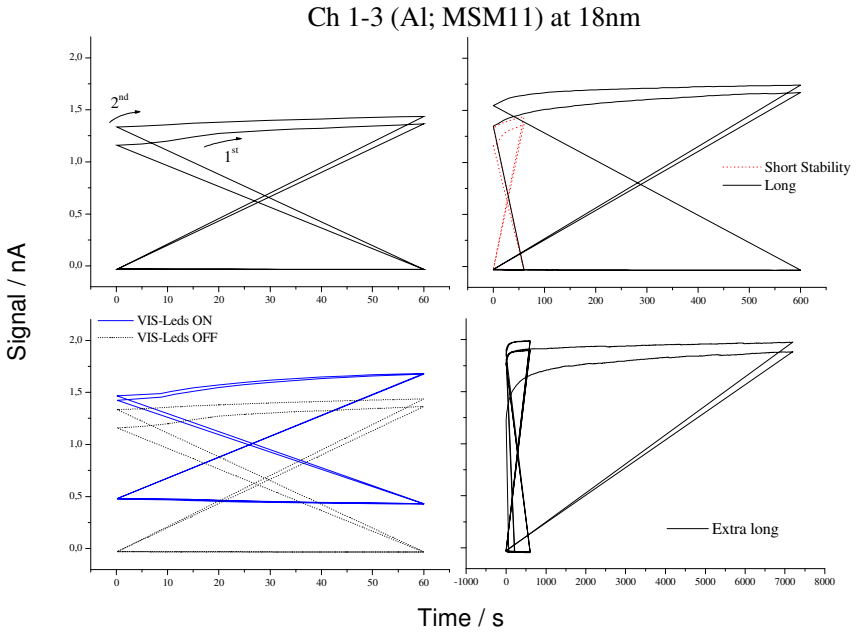

Figure 3. Absolute signal in nano-ampere as a function of time at 18 nm.

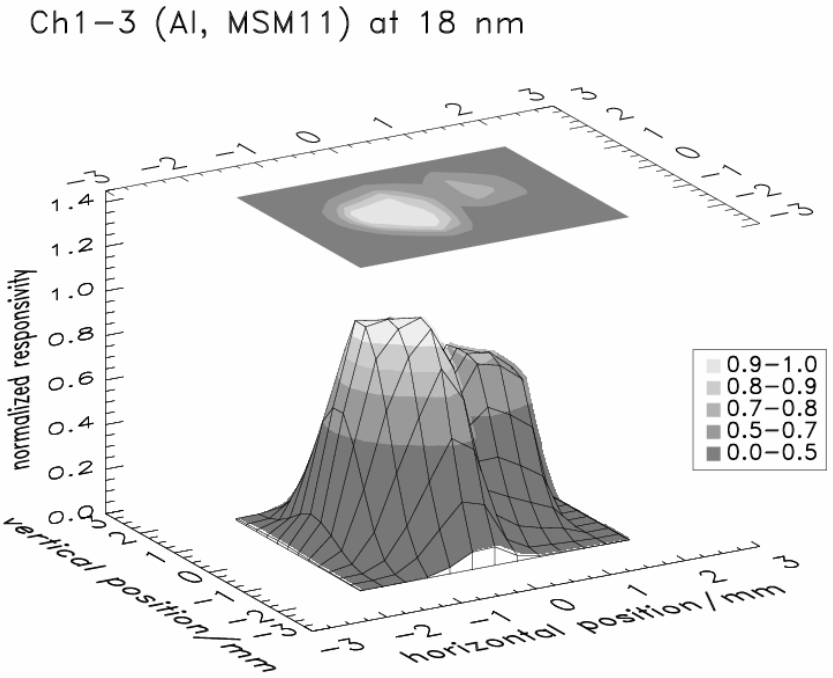

Figure 4. Homogeneity of responsivity (3-D representation) at 18 nm wavelength.

2.2 Channel 1-4 (Head 1 ; Channel 4: Zr, AXUV20D)

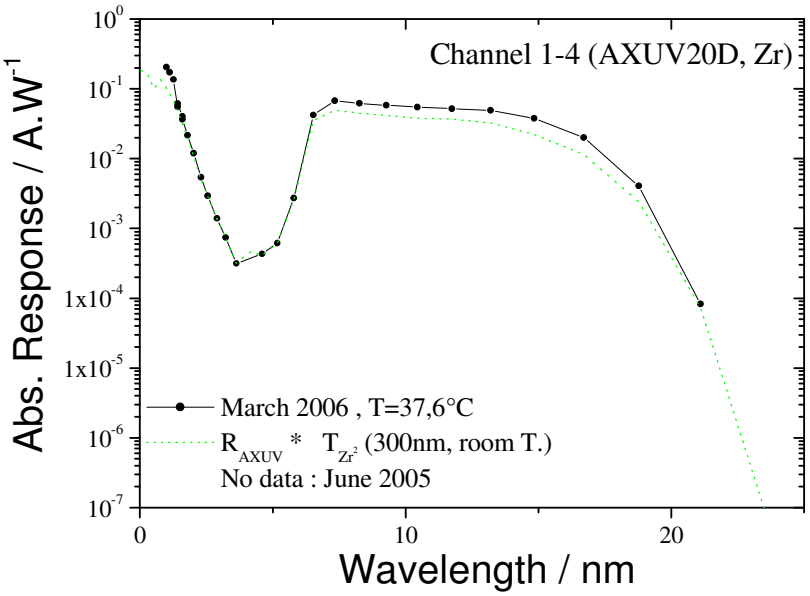

Figure 5. Absolute spectral responsivity (in A/W) of channel 1-4 between 1nm and 25 nm. For comparison, the dotted line represents the model used in the LYRA radiometric model (detector R x Filter T). Note that the Zr filter thickness is 300nm (around 150nm for MSM channels).

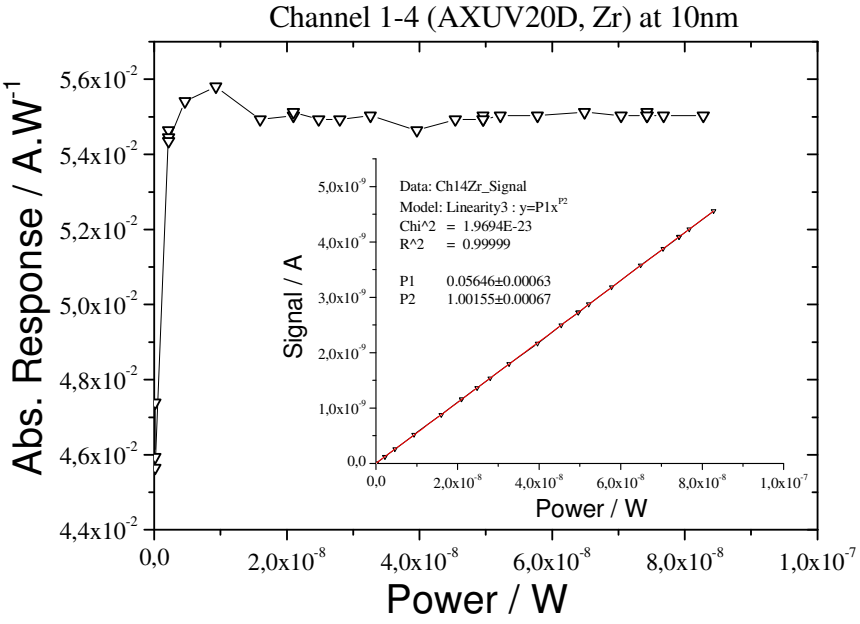

Figure 6. Flux linearity of channel 1-4 (Response vs. incident power) at 10nm. The inset shows the photocurrent vs incident power with the fitted function $I=aP^b$.

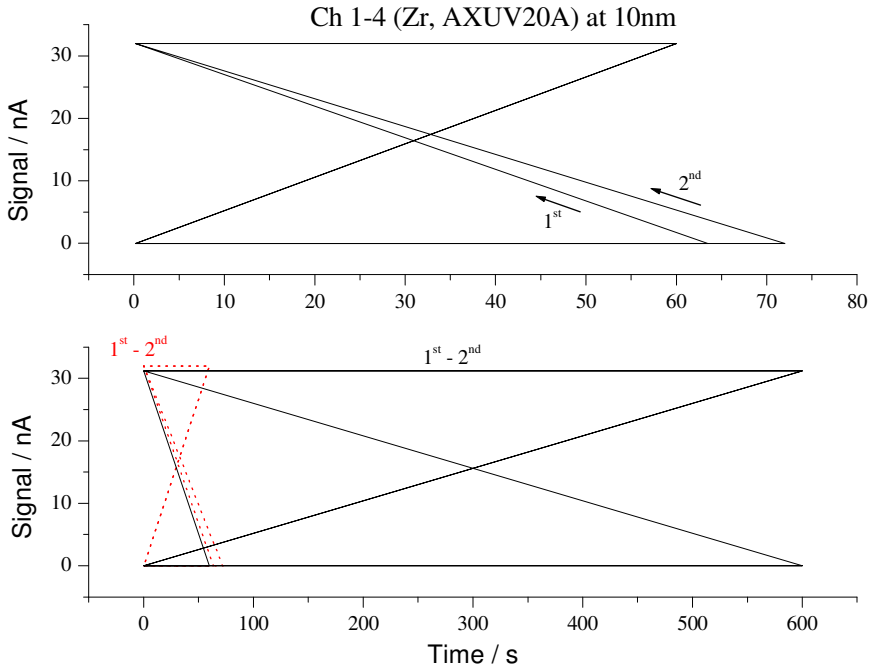

Figure 7. Absolute signal in nano-ampere as a function of time at 10 nm.

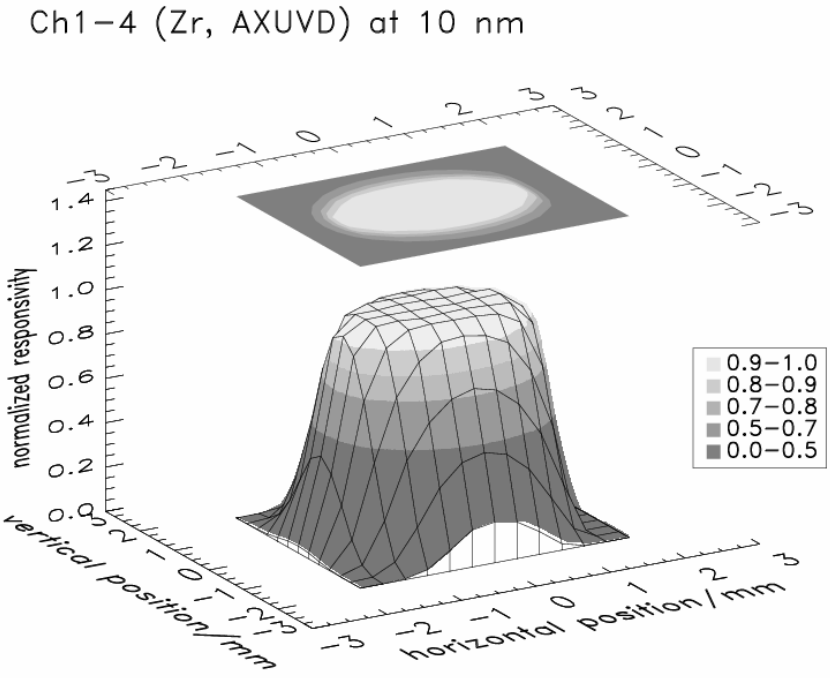

Figure 8. Homogeneity of responsivity (3-D representation) at 10 nm wavelength.

2.3 Channel 2-3 (Head 2 ; Channel 3: Al, MSM15)

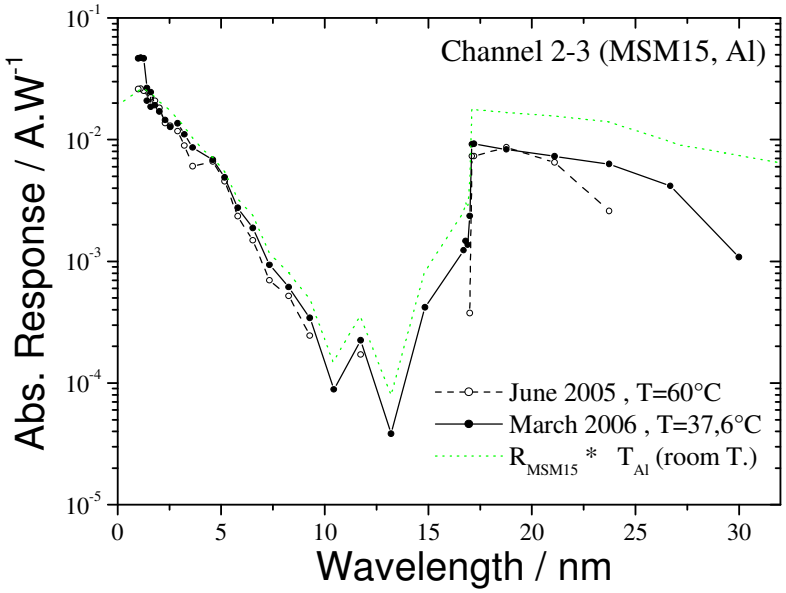

Figure 9. Absolute spectral responsivity (in A/W) of channel 2-3 between 1nm and 30 nm. For comparison, the dotted line represents the model used in the LYRA radiometric model (detector R x Filter T) and the open circle the calibrated data from June 2005 campaign.

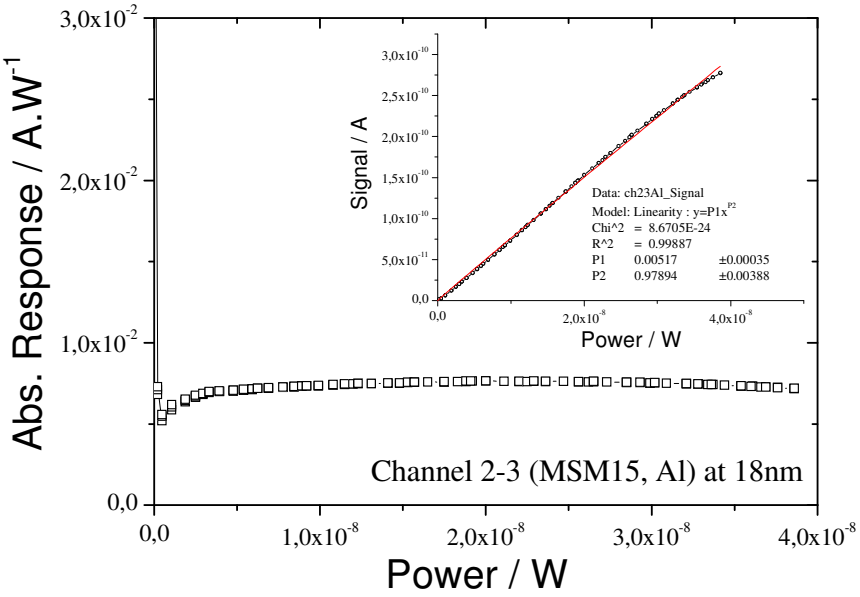

Figure 10. Flux linearity of channel 2-3 (Response vs. incident power) at 18nm. The inset shows the photocurrent vs incident power with the fitted function $I=aP^b$.

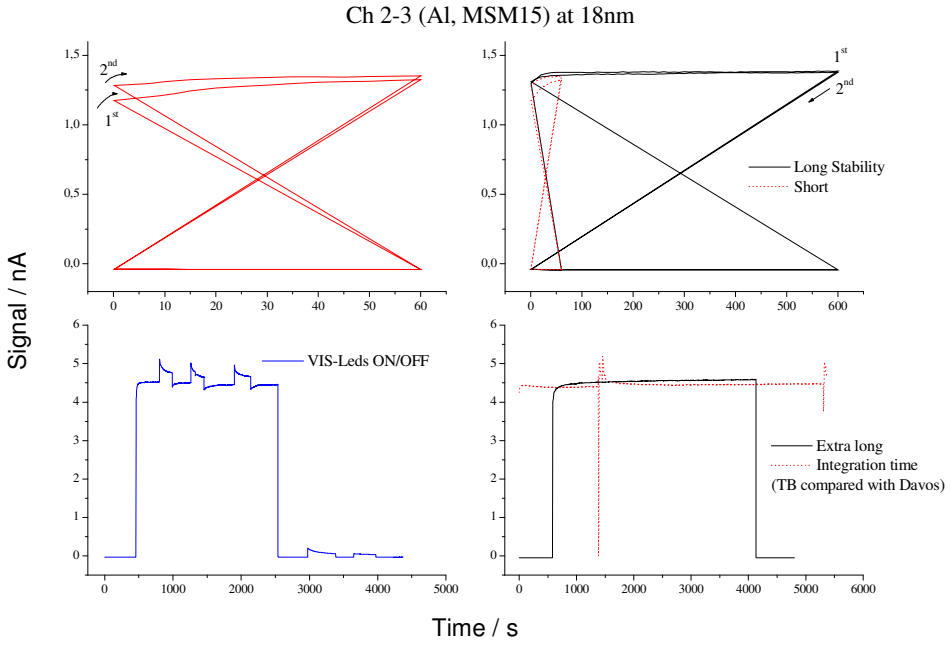

Figure 11. Absolute signal in nano-ampere as a function of time at 18 nm.

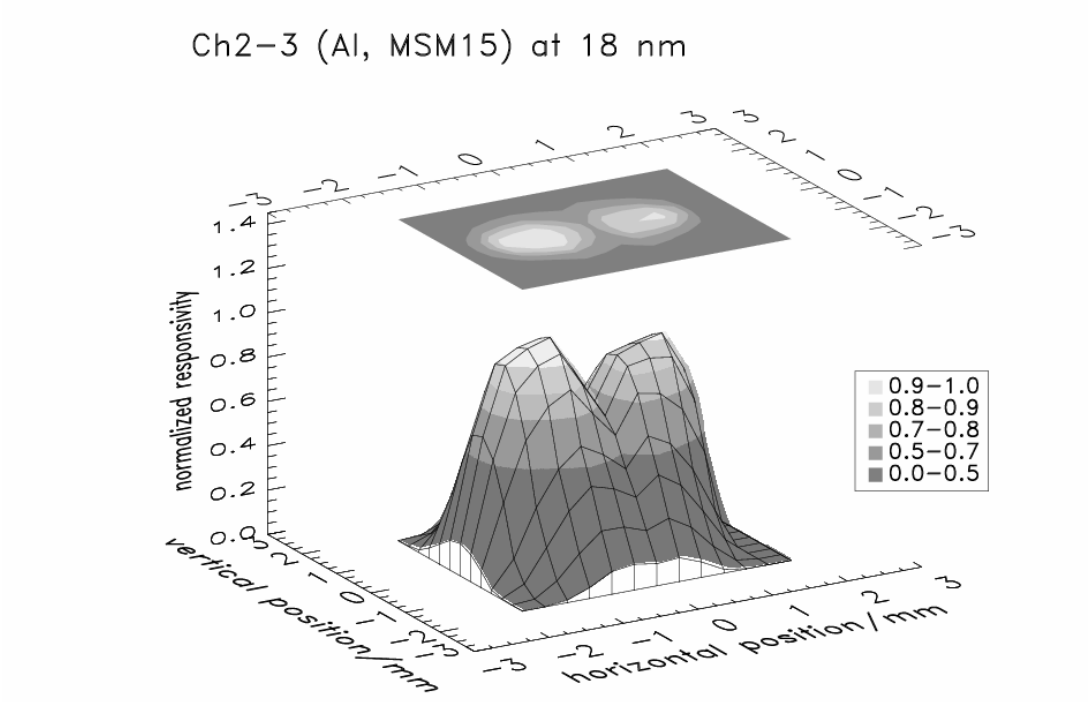

Figure 12. Homogeneity of responsivity (3-D representation) at 18 nm wavelength.

2.4 Channel 2-4 (Head 2 ; Channel 4: Zr, MSM19)

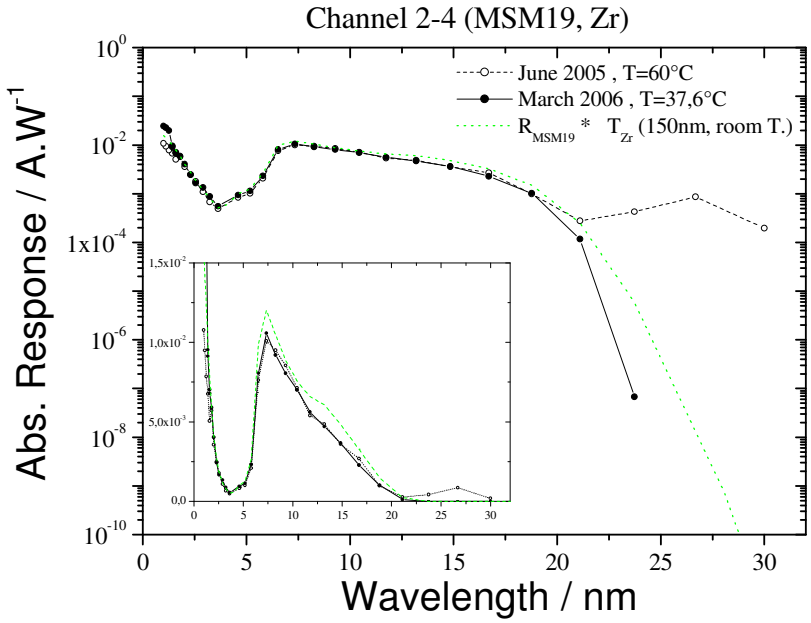

Figure 13. Absolute spectral responsivity (in A/W) of channel 2-4 between 1nm and 30 nm. For comparison, the dotted line represents the model used in the LYRA radiometric model (detector R x Filter T) and the open circle the calibrated data from June 2005 campaign. The inset shows the same in linear scale.

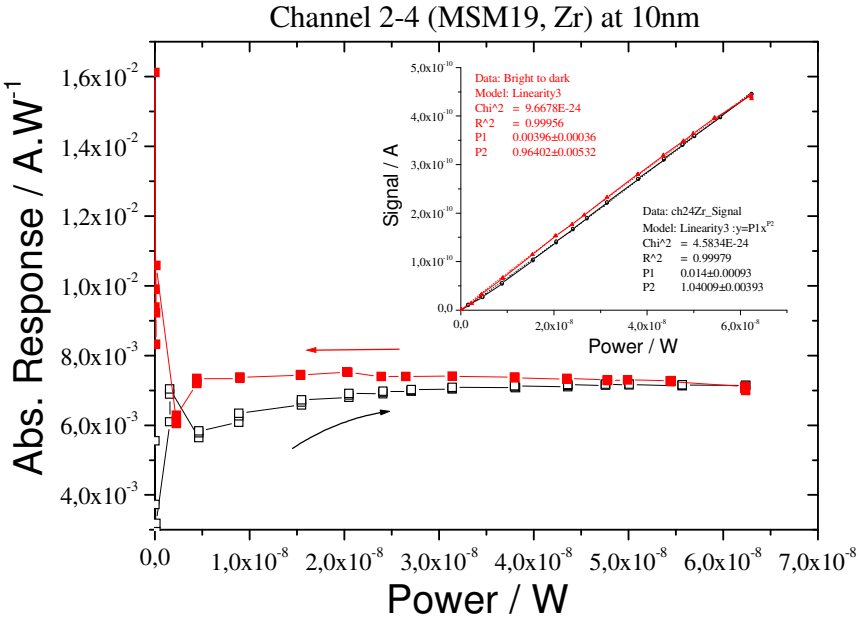

Figure 14. Flux linearity of channel 2-4 (Response vs. incident power) at 10nm. The inset shows the photocurrent vs incident power with the fitted function $I=aP^b$.

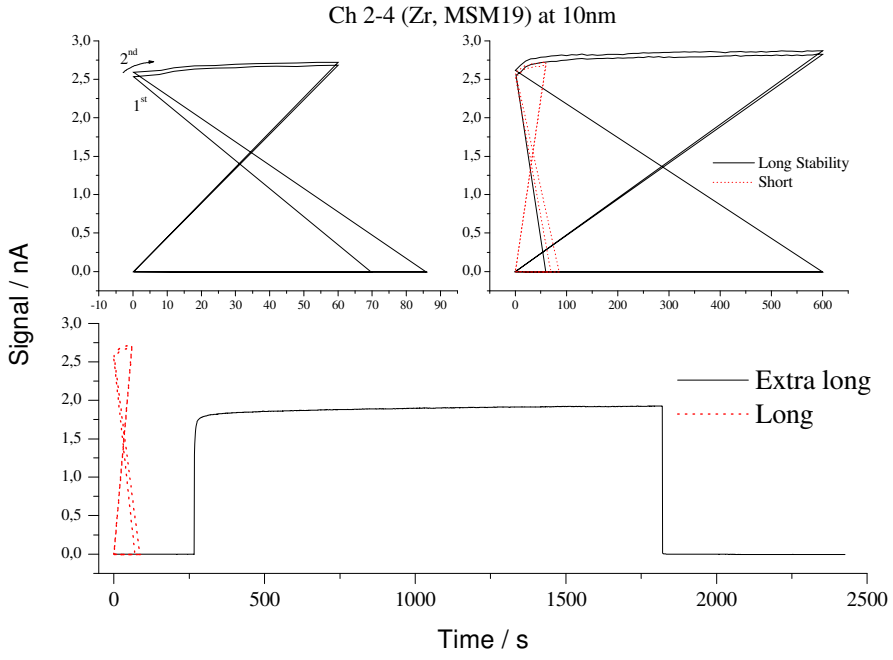

Figure 15. Absolute signal in nano-ampere as a function of time at 10 nm.

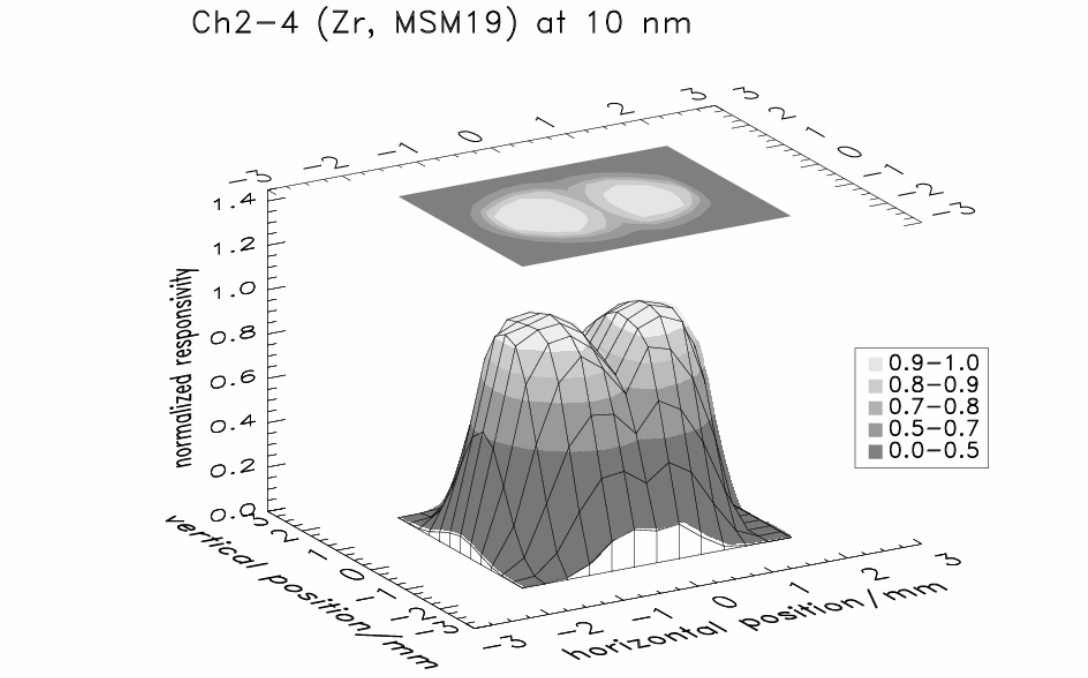

Figure 16. Homogeneity of responsivity (3-D representation) at 10 nm wavelength.

2.5 Channel 3-3 (Head 3 ; Channel 3: Al, AXUV20B#59)

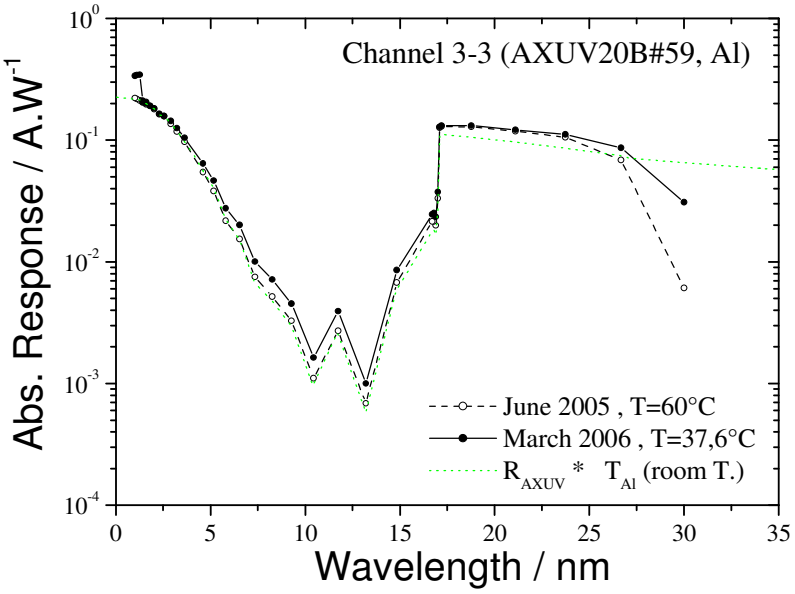

Figure 17. Absolute spectral responsivity (in A/W) of channel 3-3 between 1nm and 30 nm. For comparison, the dotted line represents the model used in the LYRA radiometric model (detector R x Filter T) and the open circle the calibrated data from June 2005 campaign.

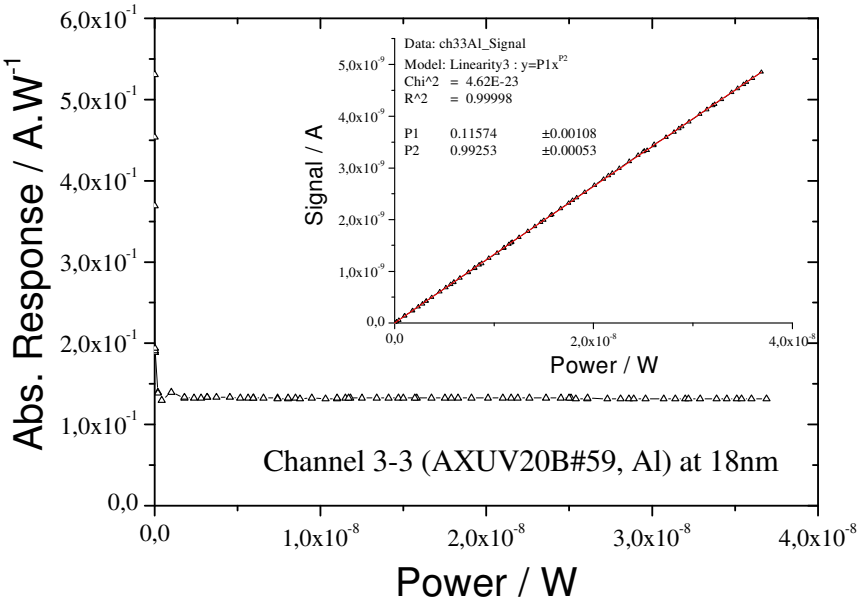

Figure 18. Flux linearity of channel 3-3 (Response vs. incident power) at 18nm. The inset shows the photocurrent vs incident power with the fitted function $I=aP^b$.

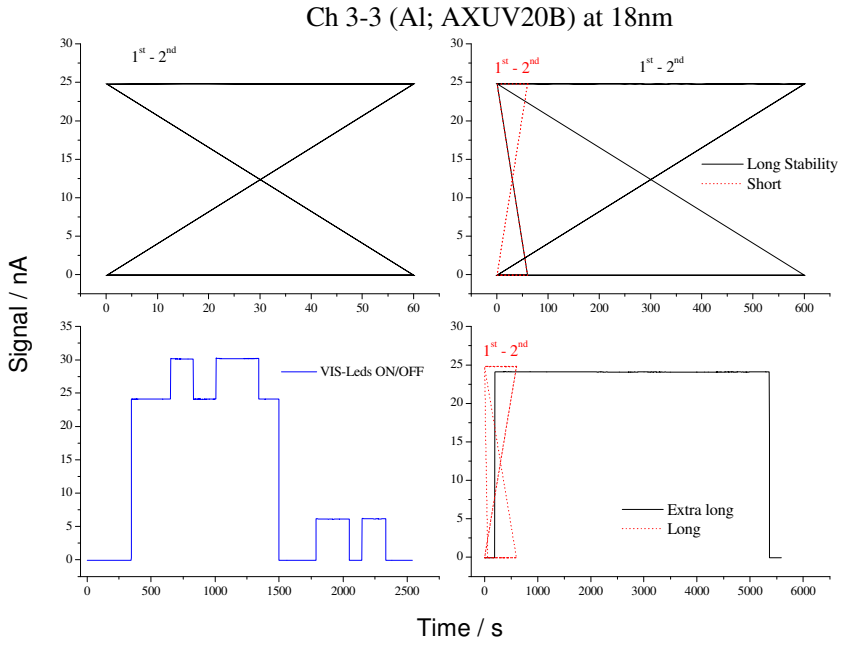

Figure 19. Absolute signal in nano-ampere as a function of time at 18 nm.

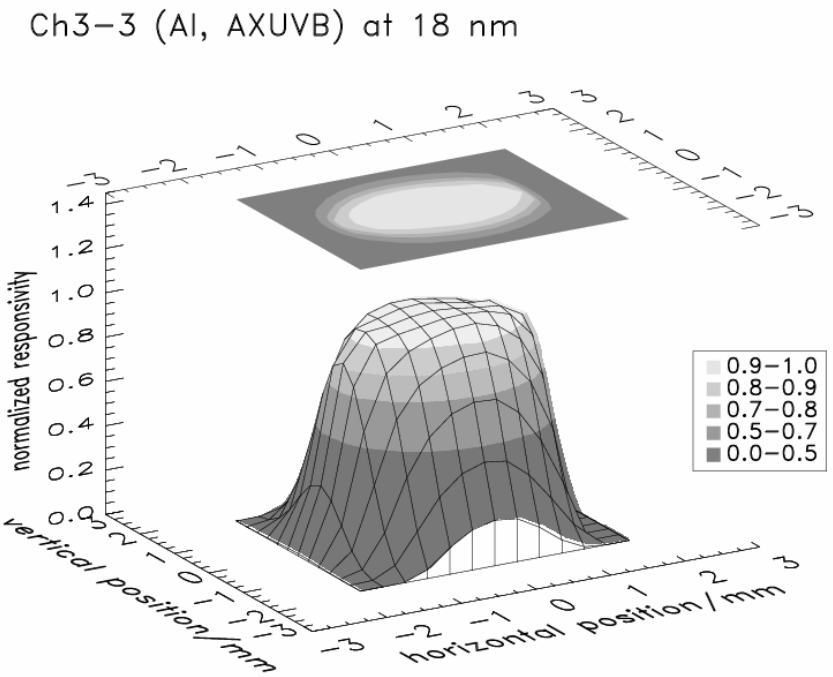

Figure 20. Homogeneity of responsivity (3-D representation) at 18 nm wavelength.

2.6 Channel 3-4 (Head 3 ; Channel 4: Zr, AXUV20C#44)

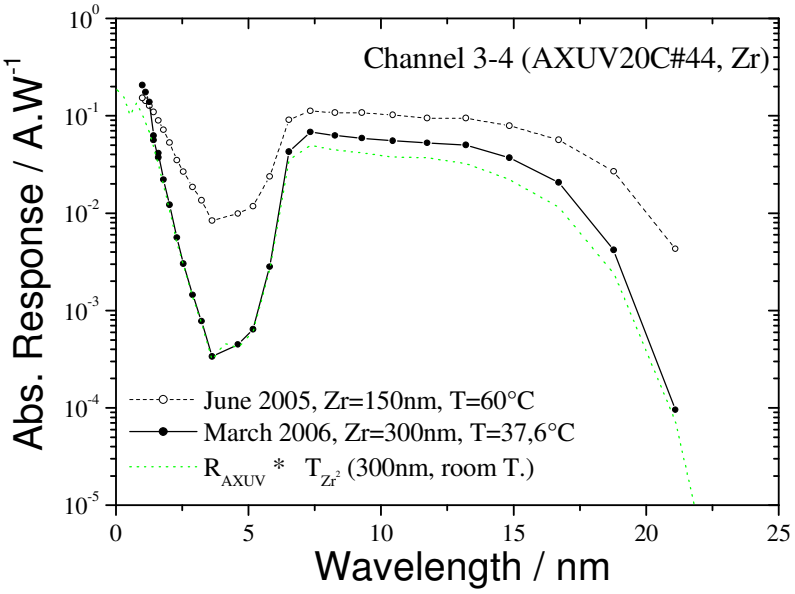

Figure 21. Absolute spectral responsivity (in A/W) of channel 3-4 between 1nm and 30 nm. For comparison, the dotted line represents the model used in the LYRA radiometric model (detector R x Filter T) and the open circle the calibrated data from June 2005 campaign. **Note that the Zr filter thickness is 300nm (150nm during June 2005' campaign)**.

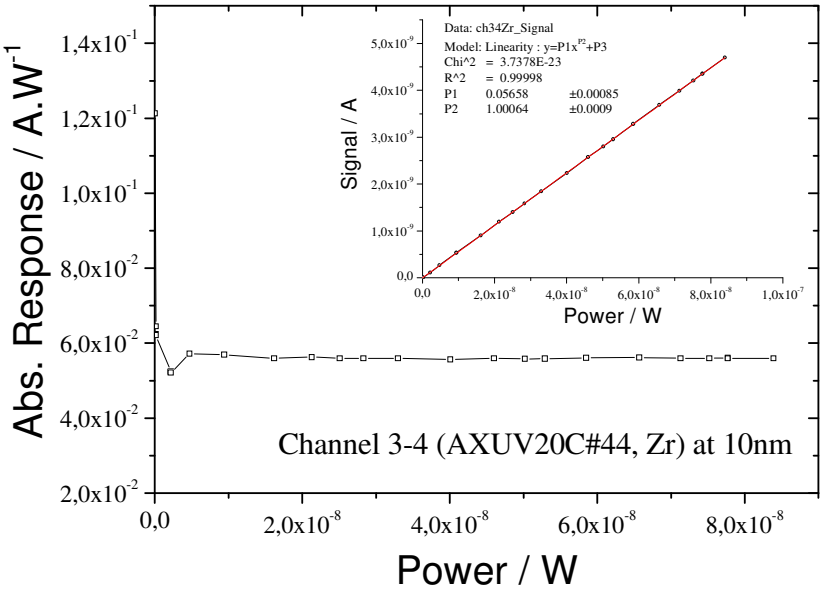

Figure 22. Flux linearity of channel 3-4 (Response vs. incident power) at 10nm. The inset shows the photocurrent vs incident power with the fitted function $I=aP^b$.

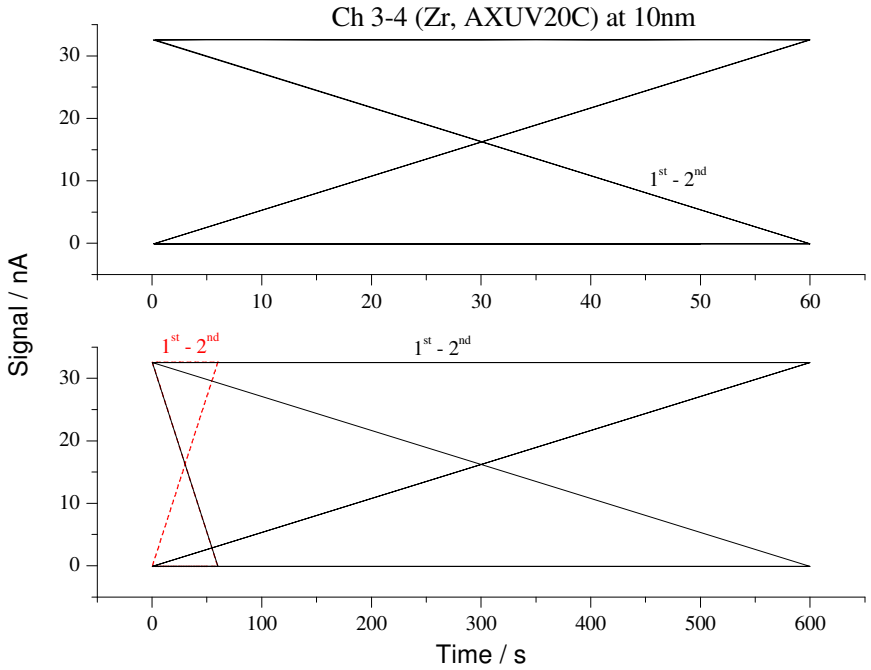

Figure 23. Absolute signal in nano-ampere as a function of time at 10 nm.

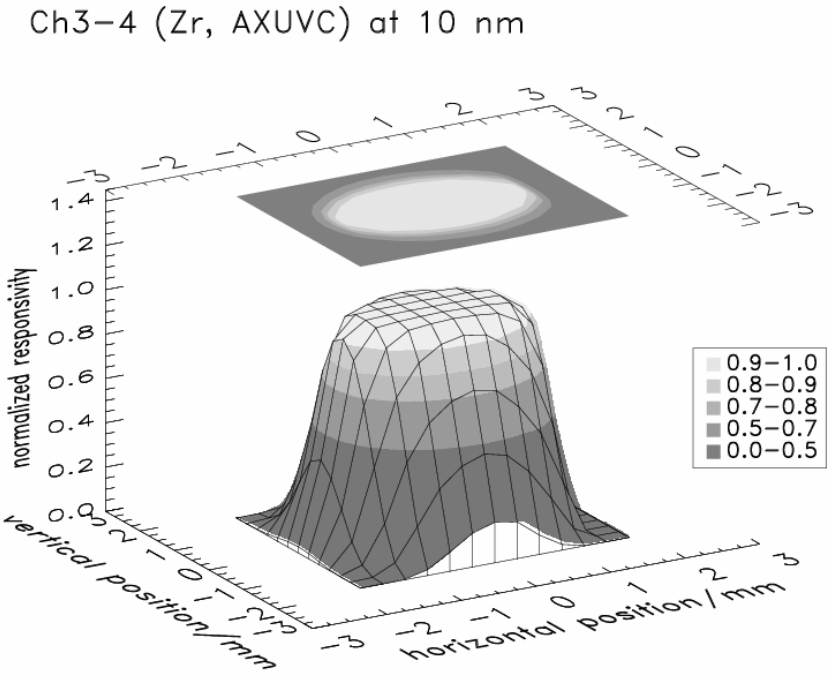

Figure 24. Homogeneity of responsivity (3-D representation) at 10 nm wavelength.

2.7 Al channels (1-3; 2-3; 3-3)

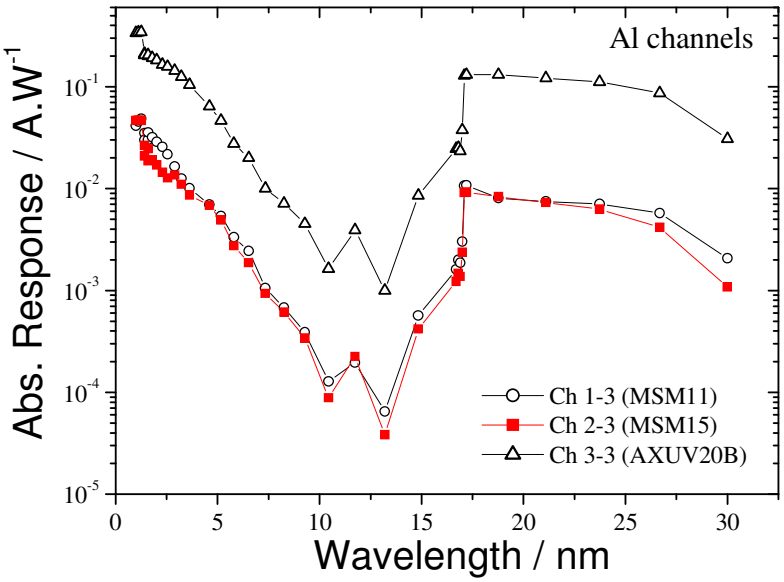

Figure 25. Absolute spectral responsivity (in A/W) of Al channels between 1nm and 30 nm for comparison.

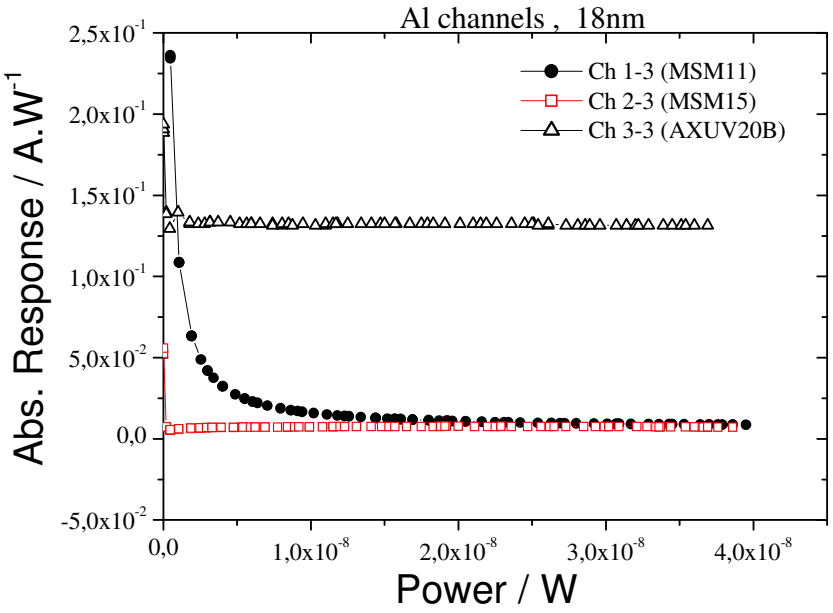

Figure 26. Flux linearity of Al channels (Response vs. incident power) at 18nm.

2.8 Zr channels (1-4; 2-4; 3-4)

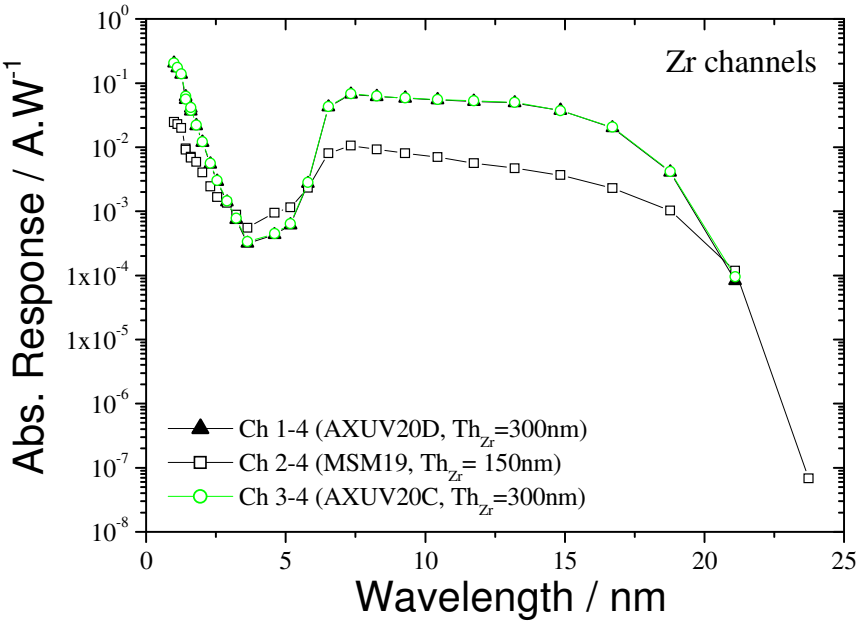

Figure 27. Absolute spectral responsivity (in A/W) of Zr channels between 1nm and 25 nm for comparison.

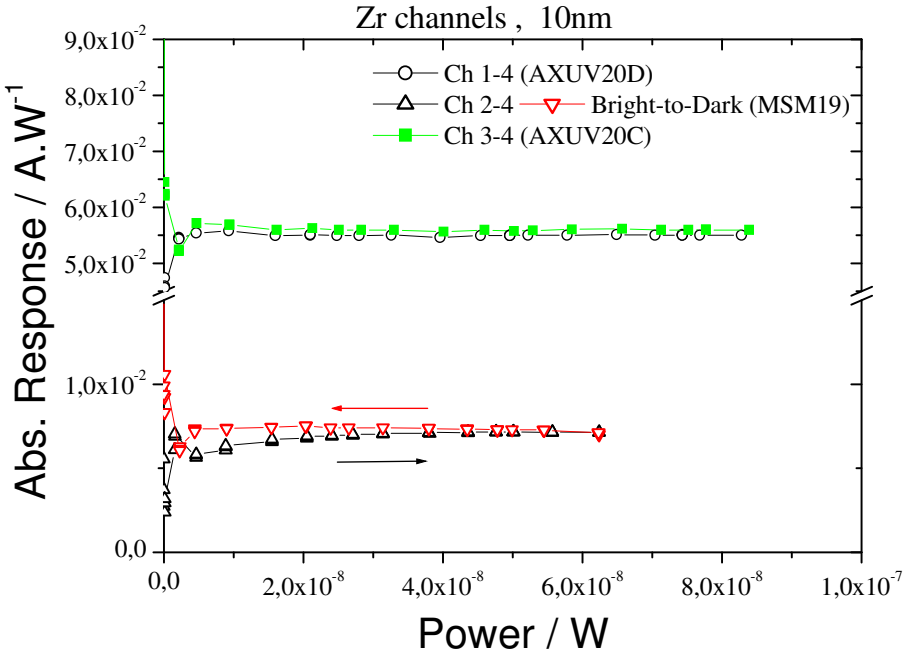

Figure 28. Flux linearity of Zr channels (Response vs. incident power) at 10nm.

Table 1 summarizes the derived results using the TIME-SEE solar spectrums. More information can be found in the updated LYRA radiometric model web site.

http://lyra.oma.be/radiometric_model/radiometric_model.php

Table 1: Expected output signals and purities (width 1-20nm for Zr and 17-80nm for Al) in LYRA channels for minimum solar activity conditions.

Expected SIGNAL and Purity			at Solar Min using Bessy GI	at Solar Min Radiometric Model
HEAD 1	**Channel 3**	**Al + MSM11**	41.2pA +NI [53.5%] ---	73.4pA [61 %]
	Channel 4	**Zr + AXUV20D**	697.9pA [99.8%] ---	524pA [98.9%]
HEAD 2	**Channel 3**	**Al + MSM15**	37.5pA +NI[55.5%] 56.8pA [52.6%]	93.6pA [73.4%]
	Channel 4	**Zr + MSM19**	94.4pA [99.6%] 93.4pA [98.9%]	110.5 pA [99.2%]
HEAD 3	**Channel 3**	**Al + AXUV20B (59)**	601.6pA +NI[66%] 838.7pA [69%]	804.4 pA [75.3%]
	Channel 4	**Zr + AXUV20C (44)**	708.2pA [99.8%] 1386pA [98.1%]	524.1pA [98.9%]

Here also we rather have an upper limit since not the entire UV and visible spectrum is taken into account. Note that for Al channels, I need the data from NI campaign to be compared with the radiometric model. In blue, the data from the previous calibration campaign (June 2005, T~60°C : [RD3]). Note that the Zr thickness for AXUV channels is 300nm instead of 150nm which reduced by a factor 2 the expected signal (~700pA) but increased the purity of the channel (~+0.7%).

3 CONCLUSION

Stability (signal vs time, integration time vs Leds) will be analysed in detail by ROB (noise fluctuation, SNR) in order to determine the nominal cadence and the choice of the Heads (continuously, weekly, monthly basis). The thermal noise (dark current) will be further analysed with NI data. The detectors are expected to have a positive T° coefficient of responsivity (increase of the responsivity with temperature).

As seen in the figures, the main issue is about channel 1-3 (MSM11). It doesn't look stable, not linear especially under low irradiation flux where the responsivity decreases rapidly with increasing incident light power up to 210^{-8}W. Since the flat field quality is spectrally dependent (cf. Annexe), It's expected to have a better homogeneity for the Zr than Al channels with diamond MSM detectors. Nevertheless, MSM channels (Ch1-3, Ch2-3 & Ch 2-4) are reasonably uniform at dedicated wavelength with the same sharp dip in sensitivity at the centre of the detector due to the middle Ti/Pt/Au contact.

For AXUV channels, the responsivity remains almost constant at 10 and 18nm indicating a linear response. These channels look stable (even with VISLEDs ON) and homogenous at 10 and 18nm with a small deviation of around 0.5%.

The radiometric model ($R_{detector}$*T_{filter}) overestimate the signal from MSM channels (e.g Ch1-3; Ch2-3 and Ch2-4) and underestimate the signal from AXUV channels (e.g. Ch3.3; Ch1-4 and Ch3-4). This will be analysed in detail with NI data. Possible explanation can be the non-linearity of MSM detectors (i.e the responsivity increases or decreases with the input light power), the non-stability of the detector with time and of course due to the uncertainty of the radiometric model itself (transmission of Zr^2 (150nm)≠Zr 300nm). It's difficult to compare these GI data to the previous calibration campaign (June 2005, T~60°C : [RD3]). We still need the data from NI calibration where the discrepancy looks higher for Al channels (cf Table1).

4 ANNEXE

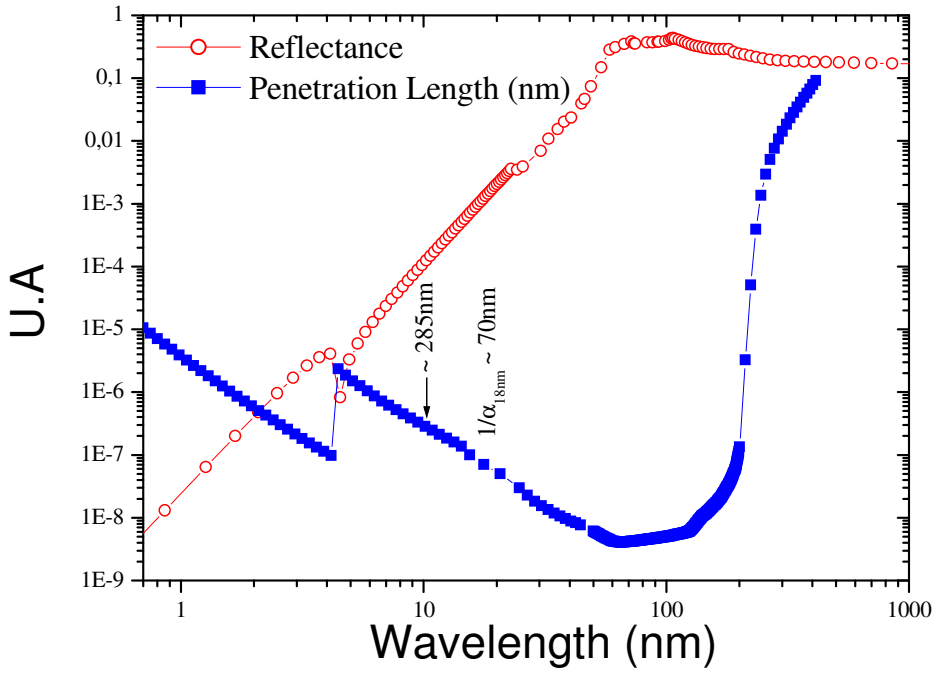

Figure 29. Reflectance and penetration length (1/α) of diamond between 1 and 400 nm.

The penetration depth is longer at 10 (1/α~285nm) than at 18nm wavelength (i.e 1/α~70nm). It's mean that the photons are more absorbed at 10nm than at 18nm. This can leads to an increase of the homogeneity of the diamond detectors (cf Fig 16).